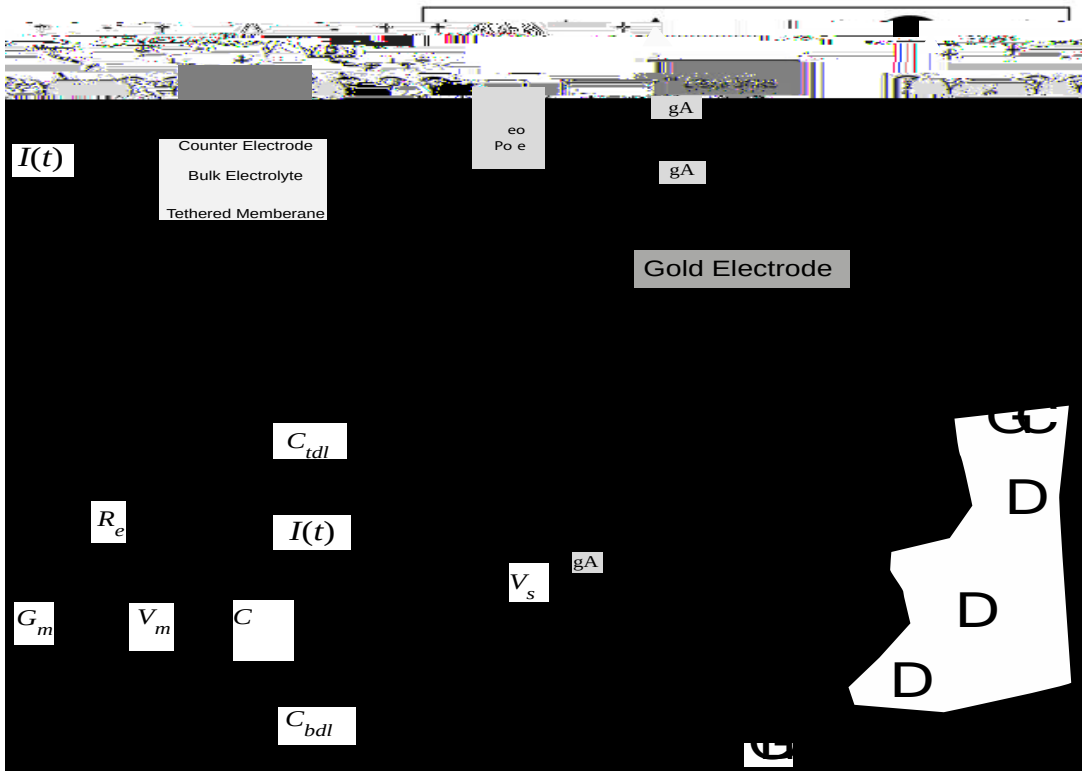


e ICS biosensor is capable of detecting femto-molar concentrations of target species including proteins, hormones, polypeptides, microorganisms, oligonucleotides, DNA segments, and polymers in cluttered electrolyte environments [10-12]. is remarkable detection ability is achieved using engineered receptor cites connected to mobile gA monomers and biotinylated lipids in the tethered membrane, refer to Figure 1. By measuring the dynamics of the membrane conductance, the concentration of a speci c analyte can be estimated. In reference to Figure 1, the mobile gA monomer is tethered to a biological receptor such as a nucleotide or antibody which binds to speci c target species. In the neighbourhood of the mobile gA, a tethered monolayer lipid is present with the tethered receptor present in contact with the analyte solution. When the receptor binds to the analyte, the mobile gA monomer di uses to the tethered lipid causing the conducting gA dimer to break. As an ensemble of gA dimers dissociate, the conductance of the membrane decreases. Measurement of the conductance change allows both the detection of the analyte species and a estimate of the concentration of the analyte species in cluttered environments as the receptor is designed to bind to a speci c target species. To relate the analyte concentration to changes in membrane conductance requires the use of an electrodi usive model for the analyte coupled with the surface reactions present at the tethered membrane surface. In the Materials and Methods section, we have constructed dynamic models for estimating the analyte concentration and surface reaction rates at the tethered membrane surface for estimating the analyte concentration.

To illustrate the application of the ICS, we compare the predicted membrane conductance with experimentally measured membrane conductance for the analyte species streptavidin [14] and ferritin [15]. Streptavidin provides a useful example as the binding a nity for streptavidin to biotin is extraordinarily high [16]. Analyte concentrations of 1000 pM, 100 pM, and 10 pM of streptavidin are used for experimental validation of the dynamic models presented. Streptavidin has a molecular weight of 52.8 kDa; to illustrate the detection characteristics of the ICS for larger molecules we consider ferritin which has a molecular weight of 450 kDa. Ferritin plays a central role in the transport, storage, and release of iron. It is known that ferritin concentrations increase drastically in organisms with pathogenic infections or cancer. erefore, the ability to detect such an event is helpful for rapid point-of-care diagnostics useful for patient healthcare. We consider the detection of 200 pM, 400 pM, and 600 pM concentrations of ferritin using experimental measurements from the ICS.

e paper proceeds by presenting how the ICS sensor is constructed, dynamic models, and parameter estimation in the Methods and Materials section. e Results and Discussion section illustrates the predictive accuracy of the dynamic models developed in the Methods and Materials section for the experimental measurement of streptavidin and ferritin. Closing remarks are provided in the Conclusion section.

## Methods and Materials

In this section the formation and predictive models of the ICS biosensor are presented. Note that the models presented in this section can be considered as extensions to the models presented for

the BIACORE surface plasmon resonance optical system and sandwich assay lateral ow bio-reactors [17-19].

## Ion channel switch biosensor construction

e construction and formation of the ICS biosensor can be found in [7,20,21], for completeness the experimental setup of the ICS is presented below.

e ICS is supported by a 1×25×75 mm polycarbonate slide onto which is patterned a 100 nm vacuum magnetron sputtered gold electrode array possessing six 0.7×3 mm active areas of membrane each of which is enclosed in a ow cell with a common gold return electrode. e sputtered gold surface is immersed in an ethanol solution containing the tethering species comprised of tethered gA monomers (tether-gA), membrane spanning lipids (MSLOH), biotinylated membrane spanning lipid (MSLB), and half membrane spanning lipids (DLP). e chemical structures of tether-gA, MSLOH, MSLB and DLP are given in Figure 1. e gold surface is immersed in the tethering solution for a period of 10 min. Following an alcohol rinse, 5

respectively. As a result of the spacers used in the ICS, it is likely that the di usion in the neighbourhood of the bioelectronic interface satis es the subdi usion process such that $\langle x^2 \rangle$ tα. e detection of this subdi usion process is well known for solid electrode to electrolyte interfaces and can be detected by measuring the frequency response of the interface, refer to [5,27]. If the interface satis es a constant-phase-element (CPE) model, then subdi usion is present suggesting that electrode e ects from surface roughness, electrode porosity, and electrode geometry are non-negligible. In the time-domain, fractional calculus is used to represent the current-voltage relationship of the bioelectronic interface [28,29] (Table 1).

e governing equations of the tethered membrane system are given by:

$$\begin{aligned}
\frac{dV_m}{dt} &= \left(\frac{1}{C_m R_e} - \frac{G_m}{C_m}\right)V_m - \frac{1}{C_m R_e}V_{dl} - \frac{1}{C_m R_e}V_S, \\
\frac{dV_m}{dt} &= \left(\frac{1}{C_m R_e} - \frac{G_m}{C_m}\right)V_m - \frac{1}{C_m R_e}V_{dl} - \frac{1}{C_m R_e}V_S, \\
\frac{d\,V_{dl}}{dt} &= \frac{1}{C_{dl} R_e}V_m - \frac{1}{C_{dl} R_e}V_{dl} - \frac{1}{C_{dl} R_e}V_S, \\
\hat{I} &= \frac{1}{R_e}(V_S - V_m - V_{dl}),
\end{aligned} \tag{1}$$

where $C_{dl}$ is the total capacitance of $C_{tdl}$ and $C_{bdl}$ in series, α is the anomalous di usion parameter in the range of $0<\alpha\leq 1$. Note if α=1 then standard di usion applies at the bioelectronic interface. Given $V_S(t)$, and the static circuit parameters $C_{tdl}, C_{bdl}, R_e, C_m$ and di usion parameter α, the membrane conductance $G_m$ can be estimated from the measured current I(t).

Using (1) with the measured current I(t) to estimate $G_m$ is computationally prohibitive for arbitrary waveforms as a result of the fractional order di erential operator in (1). If the electrodi usive properties of the analyte are not of interest to the experimentalist, or if the analyte is uncharged then the drive potential $V_s t$ can be engineered to allow straightforward estimation of $G_m$. If a sinusoidal drive potential $V_S(t) = V_O \sin(\omega t)$ with radial frequency $\omega = 2\pi f$ and magnitude $V_o$ is applied, the computation of I can be done using a set of algebraic equations. Using the sinusoidal drive potential and converting (1) into the complex domain using the Laplace transform, the current is given by $\hat{I}(\omega) = V_O / Z(\omega)$ where

e

$n \; D^A \; c^A \quad (t)$ in $_{surf}$,

$(t) \quad c^A(f_1 B \quad f_2 C \quad f_6 D) \quad r_1 W \quad r_2 X \quad r_6 Z\big|_{surf}$,

$c^A \quad c_o^A$ in $_{in}$, $n \; J^A \quad 0$ otherwise (5)

In (5), $A_o$ is the analyte concentration at the inlet, and ξ(t) is the surface ux of analyte species c^A resulting from the chemical reactions (4). Given the time-scale of the conductance measurements is seconds, we assume that the velocity eld v is a fully developed laminar ow with a parabolic velocity pro le given by:

$$v(z) \quad (\frac{6Q}{L_w h})(\frac{z}{h})(1 \quad \frac{z}{h}),$$

ferritin computed using (3a) and (6) with boundary conditions (5) and parameters estimated from (8) are in excellent agreement with the experimentally measured conductance. Note that the conductance is estimated using (2) with the drive potential having a magnitude of 20 mV.

Figure 3 presents the numerically estimated and measured conductance of the ICS for the detection of streptavidin for known concentrations of 1000 pM, 100 pM, and 10 pM. As seen in Figure 3, the experimentally measured and numerically predicted conductance are in excellent agreement. Note that for low analyte concentrations, the di usive properties of the analyte greatly in uence the population of gA dimers on the surface of the ICS. As seen from Figure 3, using the advection-di usion PDE coupled with the surface reaction allows an accurate estimate of analyte concentrations of pM concentration. By adjusting the number of binding cites and ow rate, it is possible to use the ICS to detect femto-molar concentrations of species [11,12].

e selection of the number of binding cites and ow rate optimal for detecting a certain concentration of analyte species can be done using (3a) and (6) with boundary conditions (5).

To illustrate the detection capability of the ICS for large analyte molecules, we consider the detection of ferritin which has a molecular weight of 450 kDa, as compared with streptavidin with a molecular weight of 52.8 kDa. Note that for the detection of ferritin, biotinylated antibody receptors are added to the solution that bind to the ferritin molecules. e ferritin biotinylated antibody complexes then bind to the tethered membrane biotinylated lipid molecules. Figure 4 presents the numerically estimated and measured conductance of the ICS for the detection of ferritin for known concentrations of 200 pM, 400 pM, and 600 pM. As seen in Figure 3, the experimentally measured and numerically predicted conductance are in excellent agreement.

What is the lower limit of analyte concentration that could be measured using the ICS? Since the detection mechanism of the ICS is dependent on detecting changes in membrane conductance, the question is equivalent to asking when is

4. Cranfeld CG, Cornell BA, Grage SL, Duckworth P, Carne S, et al. (2014) Transient potential gradients and impedance measures of tethered bilayer lipid membranes: pore-forming peptide insertion and the effect of electroporation. Biophys J 106: 182-189.

5. Heinrich F, Ng T, Vanderah DJ, Shekhar P, Mihailescu M, et al. (2009) A new lipid anchor for sparsely tethered bilayer lipid membranes. Langmuir 25: 4219-4229.

6. McGillivray DJ, Valincius G, Vanderah DJ, Febo-Ayala W, Woodward JT, et al. (2007) Molecular-scale structural and functional characterization of sparsely tethered bilayer lipid membranes. Biointerphases 2: 21-33.

7. Cornell BA, Braach-Maksvytis VL, King LG, Osman PD, Raguse B, et al. (1997) A biosensor that uses ion-channel switches. Nature 387: 580-583.

8. Raguse B, Braach-Maksvytis V, Cornell B, King L, Osman P, et al. (1998) Tethered lipid bilayer membranes: Formation and ionic reservoir characterization. Langmuir 14: 648-659.

9. Prashar J, Sharp P, Scarffe M, Cornell B (2007) Making lipid membranes even tougher. Journal of Materials Research 22: 2189-2194.

10. Moradi-Monfared S, Krishnamurthy V, Cornell B (2012) A molecular machine biosensor: Construction, predictive models and experimental studies. Biosens Bioelectron 34: 261-266.

11. Krishnamurthy V, Monfared S, Cornell B (2010) Ion-channel biosensors Part I: Construction, operation, and clinical studies. IEEE Transactions on Nanotechnology 9: 303-312.

12. Krishnamurthy V, Monfared SM, Cornell B (2010) Ion channel biosensors Part II: Dynamic modeling, analysis, and statistical signal processing. IEEE Transactions on Nanotechnology 9: 313-321.

13. Lomize AL, Orekhov VIu, Arsen'ev AS 1992 [Refnement of the spatial structure of the gramicidin A ion channel]. Bioorg Khim 18: 182-200.

14. Hendrickson WA, Pähler A, Smith JL, Satow Y, Merritt EA, et al. (1989) Crystal structure of core streptavidin determined from multiwavelength anomalous diffraction of synchrotron radiation. Proc Natl Acad Sci U S A 86: 2190-2194.

15. Theil EC (1987) Ferritin: structure, gene regulation, and cellular function in animals, plants, and microorganisms. Annu Rev Biochem 56: 289-315.

16. DeChancie J,